Support information for

Flexible perovskite homojunction with metallic ions doping for large-scale and high sensitivity X-ray detection

Jingda Zhao[a], Xin Wang[a], Yijing Ding[a], Ziyu Wei[a], Yubing Xu[a], Yuzhu Pan[a], Yuwei Li[a], Byung Seong Bae[b], Mamoru Furuta[c], Zhuoya Zhu[a], Qing Li[a], Jianming Zhou[d], Xiaobing Zhang[a] and Wei Lei[a]*.*

[a]Joint International Research Laboratory of Information Display and Visualization,

School of Electronic Science and Engineering, Southeast University, Nanjing 210096, China

[b]Department of Electronics &Display Engineering, Hoseo University, Hoseo Ro 79, Asan city, Chungnam 31499, Korea

[c]Department of Environmental Science and Engineering, Kochi University of Technology, Kami, Kochi 782-8502, Japan

[d]E_x ray Electronic Co. Ltd., Suzhou, China

E-mail:
Wei Lei: lw@seu.edu.cn
Xin Wang: xinw@seu.edu.cn

Keywords: flexible X-ray detectors, perovskite homojunction, ions doping

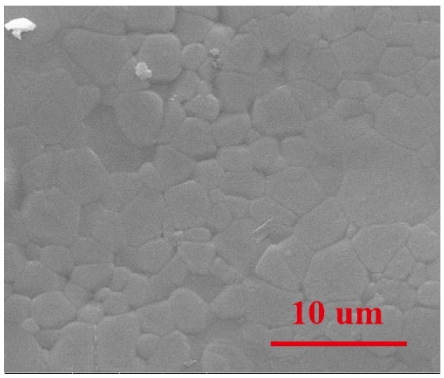

Figure S 1. Top-view SEM image of the p-n homojunction.

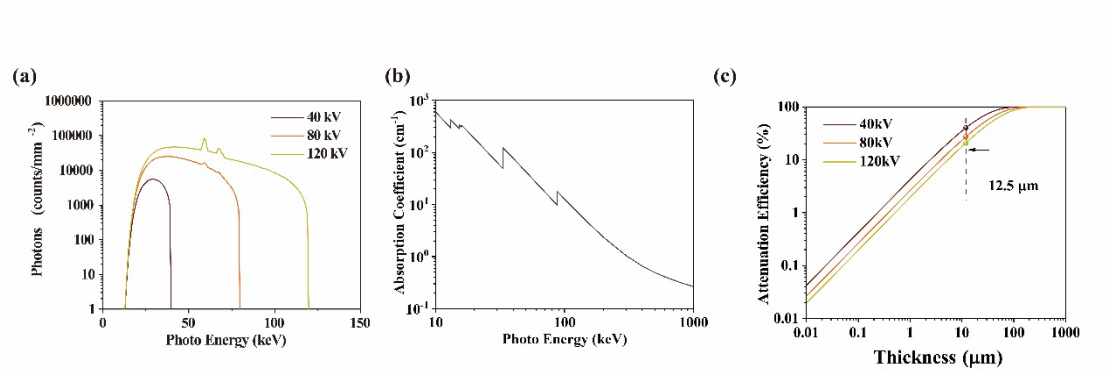

Figure S 2. (a) X-ray energy spectra of X-ray source voltage at 40, 80, and 120 kV. (b) Absorption coefficient (μ) of $MAPbI_3$ for X-rays with energy ranging from 10 to 1000 keV. (c) Calculated attenuation efficiency of $MAPbI_3$ versus the thickness of X-rays with different energies.

The energy distribution of the X-ray beam (Figure S2a) was evaluated using SPEKTR 3.0, as shown in Figure S2a, and the absorption coefficient of $MAPbI_3$ (Figure S2b) was calculated using an XCOM application. The attenuation efficiency (in case of 40 kV) of our device was calculated according to the formula $\varepsilon = \frac{\int_{0Kev}^{40KeV}(1-e^{-\mu*\rho*t})\,E}{\int_{0Kev}^{40KeV} E}$, where ρ is the material density of $MAPbI_3$ (4.16 g/cm^3), t is the thickness of our device, and E is the energy (keV) of X-ray photons. The attenuation efficiency values of our device at 40, 80, and 120kV are shown in Figure S2c.

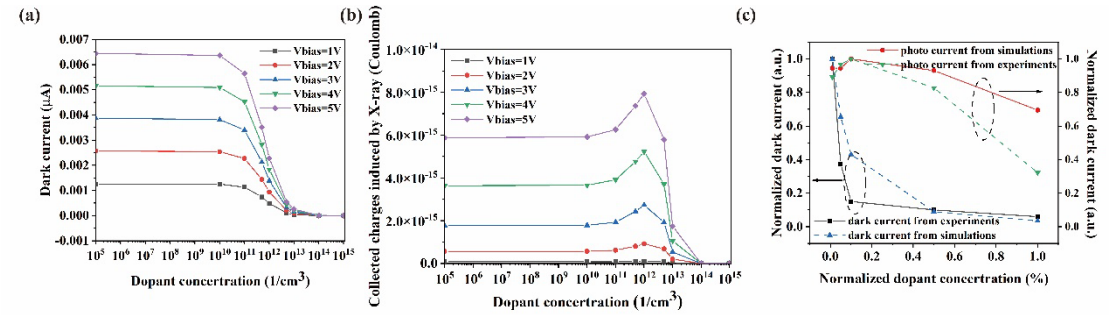

Figure S 3. Simulation results of (a) dark current and (b) photocurrent induced by X-ray with different dopant concentrations in the n-$MAPbI_3$ layer. (c) Comparison of simulation results with measured results.

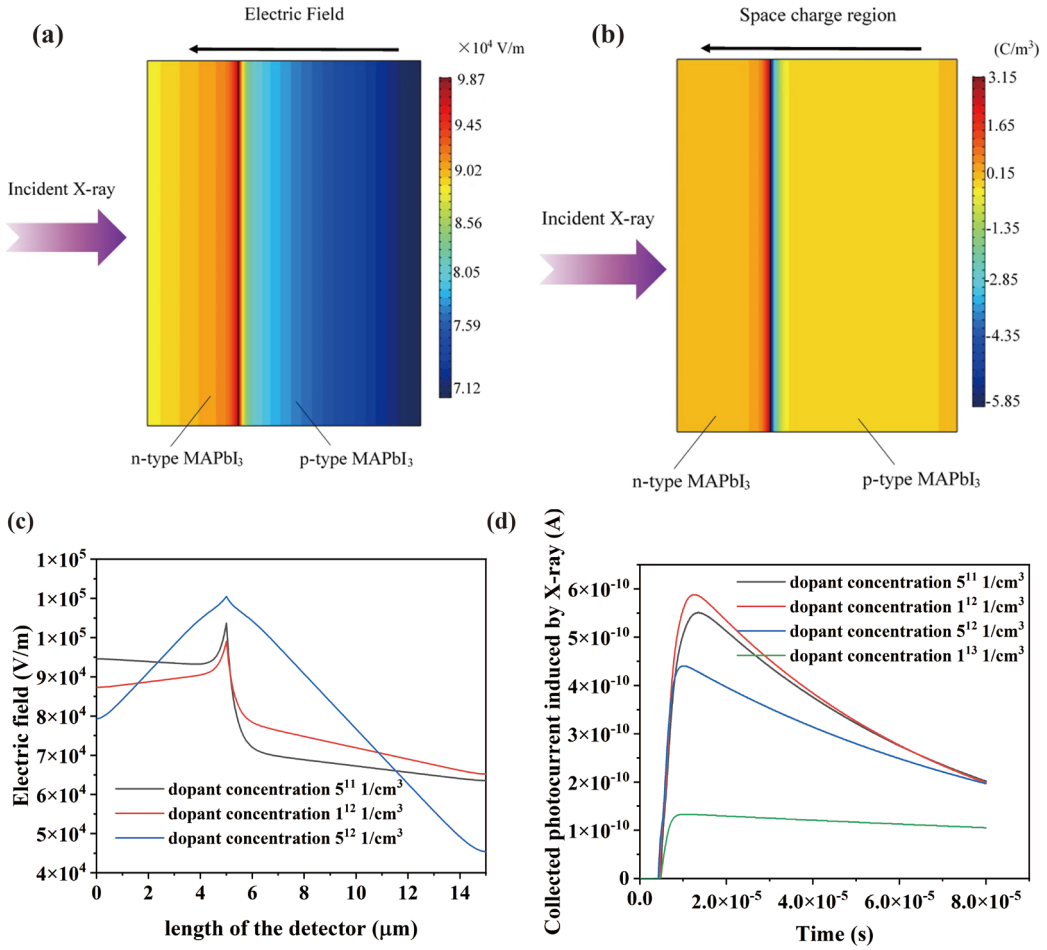

Figure S 4. Detector performance obtained from numerical simulations. (a) Electric field distribution in the perovskite homojunction. (b) Space charge density of the perovskite homojunction. (c) Electric field in the homojunction with different dopant concentrations. (d) Waveform of photocurrent collected by the electrodes.

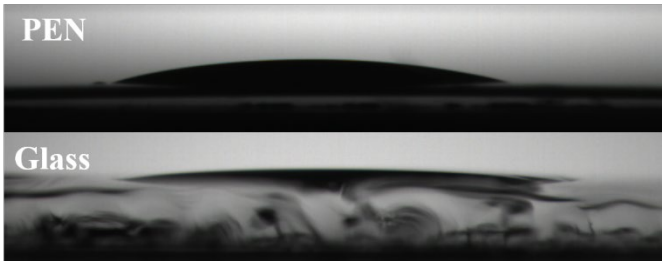

Figure S 5. Contact angle images of $MAPbI_3$ precursor dripped on PEN/ITO and Glass/ITO substrate, the substrates have been treated with ultraviolet-ozone for 10 mins.

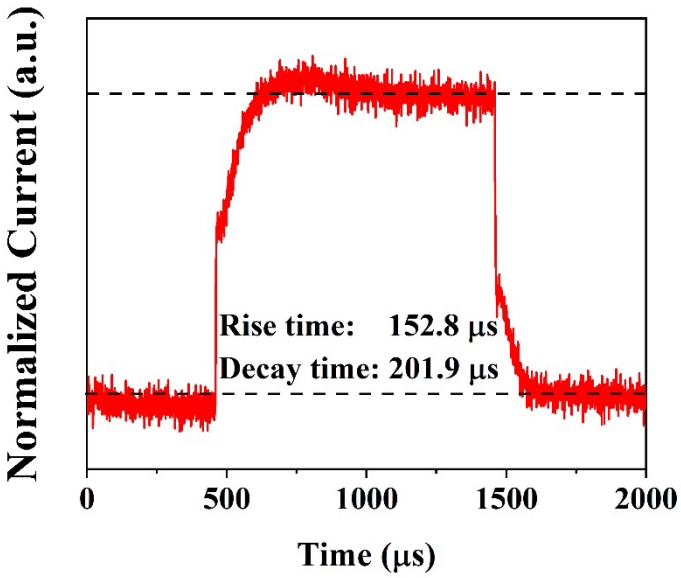

Figure S 6. Rise and decay times of the flexible X-ray detectors measured by visible light (535 nm).

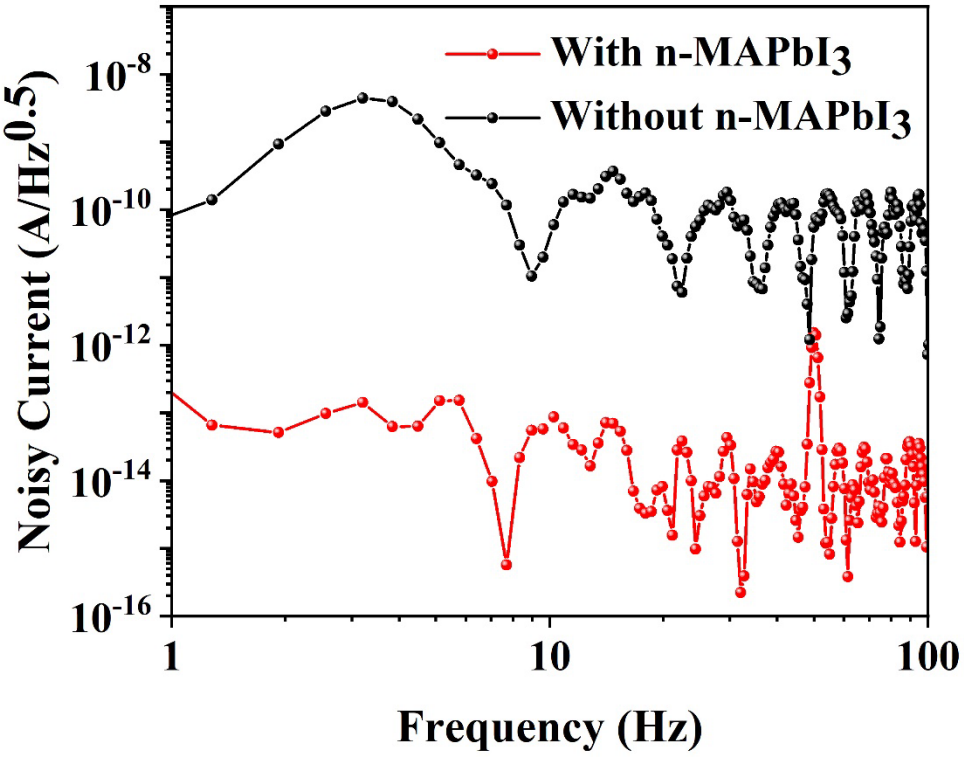

Figure S 7. Dark current noise of the device with and without the n-$MAPbI_3$ layer.

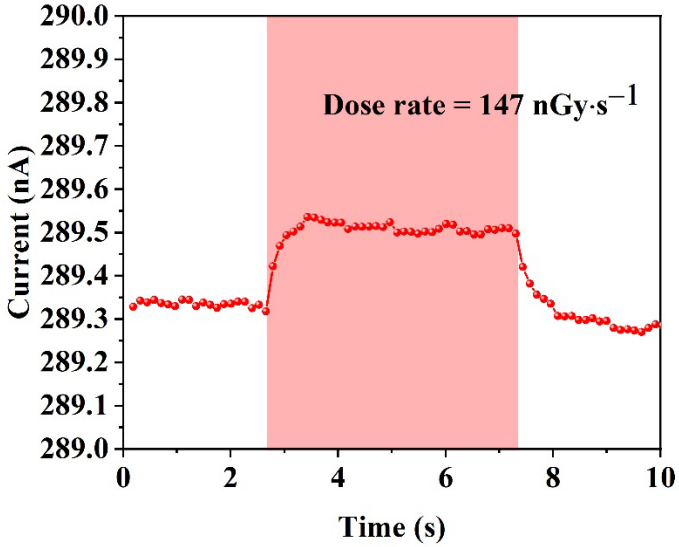

Figure S 8. X-ray response with a dose rate of 147 nGy·s^{-1}.

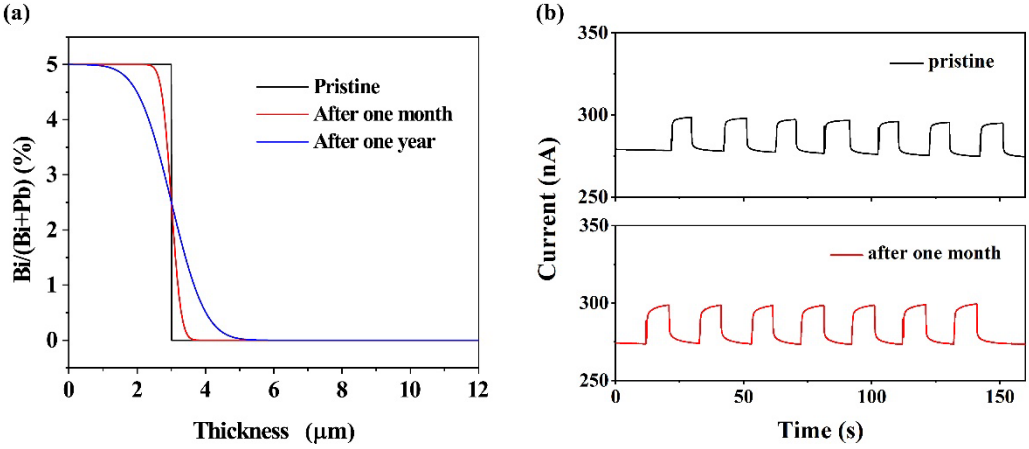

Figure S 9. (a) Simulation of Bi and Pb ion distribution in the pristine sample and the samples after one month and after one year. (b) X-ray photo response of the flexible X-ray detector in the flat condition for the pristine sample and the sample stored under ambient atmosphere with 30%–50% RH for one month.

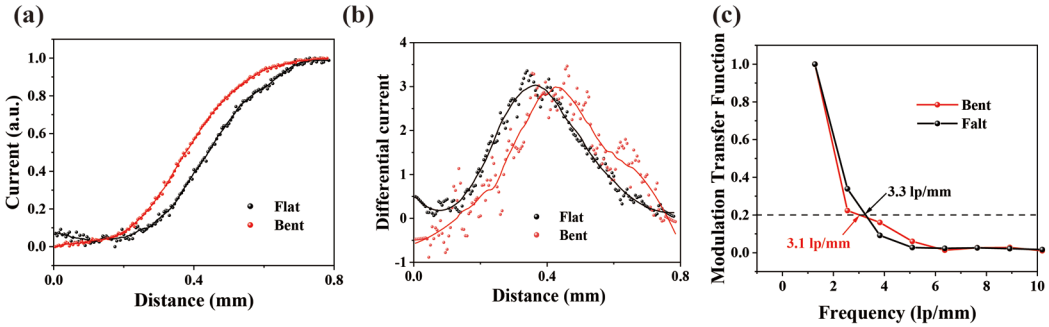

Figure S 10. (a) Function fit (line) for edge spread function of the device in flat and bent state. (b) The derived line spread function of the device under different state. (c)

Modulation transfer function of the device under flat and bent state, which is according to the Fourier transfer of the derived line spread function.

	τ_1 (μs)	τ_2 (μs)
p-$MAPbI_3$	1.91	14.89
n-$MAPbI_3$	0.44	6.40

Table S 1. PL decay curves of p- and n-$MAPbI_3$ fitted with bi-exponential function.

Device	Thickness (μm)	Bias (V)	Sensitivity ($\mu C \cdot Gy_{air}^{-1} cm^{-2}$)	LOD	Rise/Decay time	Ref.
Au/ $BA_2MA_2Pb_3I_{10}$/Au	10	5	1214@40kV	-	-/-	[1]
Au/Cs_4PbI_6/Au	8.4	10	256.2@30kV	-	-/-	[2]
Au/Cs_2TeI_6/Au	3.4	5	76.27@20 kV	0.17μGy·s^{-1}	-/-	[3]
Au/$MAPbI_3$:PCBM/Au	10	4	178@40 kV	27 μGy·s^{-1}	52/122 ms	[4]
Cr/C_{60}/BCP/$MAPbI_{0.9}Cl_{0.1}$/Cr	240	12	2204@60 kV	-	-/-	[5]
Au/$Cs_2AgBiBr_6$/Au	100	400	40@45 kV	-	-/-	[6]
Au/$CsPbBr_3$/Au	0.02	0.1	17.7@2.5 kV	-	30/27 ms	[7]
ITO/n-$MAPbI_3$/p-$MAPbI_3$/Au	12.5	1	1969@40 kV	<147nGy·s^{-1}	152.8/201.9 μs	This work

Table S 2. Comparison of key parameters of flexible perovskite X-ray detectors.

Reference

1 H. Tsai, S. Shrestha, L. Pan, H.-H. Huang, J. Strzalka, D. Williams, L. Wang, L. R. Cao and W. Nie, *Adv. Mater.*, 2022, 9.

2 C. Li, S. Zhou, J. Nie, J. Huang, X. Ouyang and Q. Xu, *Nano Lett.*, 2021, **21**, 10279–10283.

3 J. Guo, Y. Xu, W. Yang, B. Xiao, Q. Sun, X. Zhang, B. Zhang, M. Zhu and W. Jie, *ACS Appl. Mater. Interfaces*, 2021, **13**, 23928–23935.

4 A. Ciavatti, R. Sorrentino, L. Basiricò, B. Passarella, M. Caironi, A. Petrozza and B. Fraboni, *Adv. Funct. Mater.*, 2021, **31**, 2009072.

5 J. Zhao, L. Zhao, Y. Deng, X. Xiao, Z. Ni, S. Xu and J. Huang, *Nat. Photonics*, 2020,

14, 612–617.
6 H. Li, X. Shan, J. N. Neu, T. Geske, M. Davis, P. Mao, K. Xiao, T. Siegrist and Z. Yu, *J. Mater. Chem. C*, 2018, **6**, 11961–11967.
7 J. Liu, B. Shabbir, C. Wang, T. Wan, Q. Ou, P. Yu, A. Tadich, X. Jiao, D. Chu, D. Qi, D. Li, R. Kan, Y. Huang, Y. Dong, J. Jasieniak, Y. Zhang and Q. Bao, *Adv. Mater.*, 2019, **31**, 1901644.